Simultaneous PIV-LIF measurements with an sCMOS color camera using RuPhen

J. Shah[1,2*], C. Mucignat[2], I. Lunati[2], T. Rösgen[1]

1: Institute of Fluid Dynamics, Department of Mechanical and Process Engineering, ETH Zürich, Switzerland
2: Laboratory of Multiscale studies in Building Physics, Empa Dübendorf, Switzerland
*Corresponding author: jiggar.shah@empa.ch

Keywords: PIV, LIF, color camera, thermometry, heat transfer

ABSTRACT

Simultaneous velocity and temperature measurements are important in understanding the heat and momentum transfer in thermal fluid flow applications. In this work, we present a low-cost PIV-LIF system to simultaneously measure velocity and temperature fields in aqueous flows with a single color camera, a CW laser (λ_e=465 nm) and a novel dye RuPhen. The technique can also be extended to 3D LIF/3D2C PIV using a scanning light sheet. We find that the RuPhen dye is well suited due to its peak absorption in the blue, emission in the red and a strong temperature dependent emission with a sensitivity coefficient of -4%/°C. We also propose a method to use the red and green channels to correct for any laser power fluctuations. We demonstrate the technique by studying the flow past and inside a heated hollow hemisphere in a small water tunnel.

1. Introduction

The development of non-intrusive measurement techniques that aim to quantify velocity and temperature fields has been the focus of numerous studies in experimental fluid dynamics. Quantifying simultaneously temperature and velocity fields in fluid flow is extremely important for understanding the transport of heat and momentum transfer in thermal fluid flow applications. PIV (Willert & Gharib (1991), Westerweel (1997)) and LIF (Walker (1987), Coppeta & Rogers (1998)) are currently whole-field non-intrusive state-of-the-art measurement techniques that have been widely adopted in the fluid mechanics community to quantify velocity and temperature fields, respectively.

Whole-field temperature fields can be measured with fluorescent dyes or solid particles by recording changes in luminance (intensity) or chrominance (wavelength). With solid particles, the advantage is that they can also act as PIV tracers, thereby combining velocity and temperature measurements simultaneously. Particle image thermometry (PIT) involves the use of thermochromic liquid crystals (TLCs) that reflect different parts of the visible spectrum depending on temperature. The color response of these TLC particles when illuminated with a white light source can therefore be related to the temperature of the fluid (Dabiri & Gharib (1991), Dabiri (2009)). Significant progress has been made in measuring 3D temperature and velocity fields using 5 cameras by combining PIT and tomographic PIV (Schiepel et al. (2016)). Limitations of the PIT technique are the small temperature range of TLCs and the color responses's dependence on the angle between illumination and observation. Another particle-based approach to measure temperature fields is based on luminance (intensity) using temperature-sensitive particles. These particles have a fluorescence intensity (Someya et al. (2011), Vogt & Stephan (2012), Massing et al. (2016), Cellini et al. (2017)) and lifetime (phosphorescence, Aldén et al. (2011), Abram et al. (2016)) that depend on temperature. Recently, in microfluidics 3D velocity/temperature fields were acquired by Massing et al. (2018) based on luminescence lifetime of EuTTA doped particles using a scanning light sheet.

Although temperature-sensitive particle based approaches make it convenient to also use them as PIV tracers, a better spatial resolution in the temperature field, lower uncertainty, significantly lower costs, and a higher temperature range are obtained when fluorescent dyes are dissolved in the bulk fluid. Our aim is to improve upon the previous work (Shah et al. (2018)) where we use two non-toxic dyes to perform ratiometric two color - two dye (2c/2d) LIF measurements along with PIV. We consider in particular the high costs (>100k CHF) involved in using a Nd:YAG pulsed laser and a minimum of three monochrome sCMOS cameras (2 for 2c/2d ratiometric LIF, 1 for PIV). The experimental set-up for such a configuration is quite cumbersome since a pixel-to-pixel mapping of all three cameras is required, and the use of beam splitter optics halves the fluorescence signals thereby reducing the signal/noise ratio. Other limitations include the fact that since the absorption of uranine at 532nm was relatively low, a higher concentration of the dye and higher laser energies were required for single-shot temperature measurements. Also the chlorophyll dye was found to be photo-sensitive and would degrade over time. To overcome some of the limitations, we present here an innovative measurement setup to perform both velocimetry and thermometry measurements using a single camera in combination with a low-cost laser system and a novel fluorescent dye.

2. Color camera PIV-LIF

PIV measures the displacement of a constellation of tracer particles using cross-correlation to obtain the velocity field, while LIF uses temperature-dependent fluorescence emission to map the intensity to temperature using a calibration. The main idea is that these two distinct signals can be separated with the use of a color camera. Most color cameras have a Bayer pattern consisting of a color filter array (CFA) that is placed on top of the camera sensor as shown in Fig. 1a. To the author's knowledge so far only one PIV-LIF study has been performed using a color camera to quantify simultaneously velocity and temperature fields in aqueous flows. Funatani et al. (2004) used an Ar-ion laser (λ_e = 488nm), a color CCD camera, 7μm particles, and a two-color, two-dye (2c/2d) combination of RhB/Rh110 to obtain temperature fields in a buoyant plume using the ratio of red/green channels and tracer displacement in the blue channel. However, the temperature sensitivity, s, of the combination was found to be 1.7% and dependent on particle seeding density as the particles were visible in the green. Moreover, the temperature field may be prone to errors that arise due to the overlap in the Bayer filter and the emission spectra of the two dyes (2c/2d). In this work, we use the color version of the scientific CMOS sensors (sCMOS) that have the advantage of very low noise levels (1-3e-), global shutter capability, and relatively high frame rates 50-100Hz. However, the double-frame mode option for the color version of the camera is not yet available and restricted the timing of the PIV recordings. The QE and spectral curves of the color filters of the PCO, "Edge 5.5" camera are shown in Fig. 1b. To use all three RGB channels of the color camera, the aim is to therefore capture the Mie-scattering of the PIV particles in the blue, and find a suitable dye that has a peak absorption in the blue and a temperature-dependent fluorescence emission in the red/green channels. With a 2C/1D approach, the errors that arise from spectral conflicts with 2c/2d approach can also be avoided.

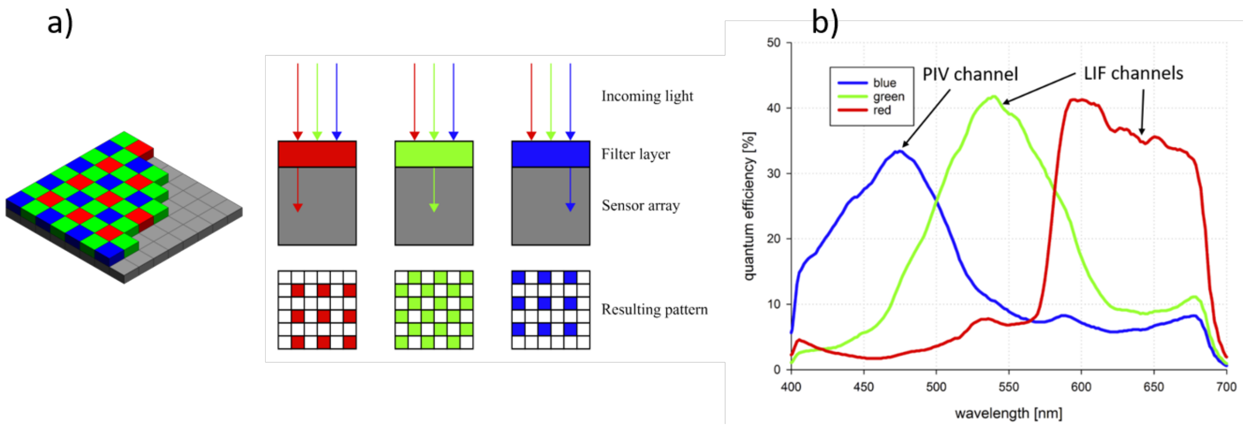

Figure 1. a) The Bayer arrangement of color filters on the pixel array of an image sensor (`https://www.wikipedia.org/wiki/Bayer_filter`) b) PCO.edge 5.5 color sensor quantum efficiency curve (adapted from https://www.pco.de/scientific-cameras/pcoedge-55/)

3. Dye selection and laser assembly

In this work, a water soluble Ruthenium based dye RuPhen (Tris(1,10-phenanthroline)ruthenium(II) chloride hydrate, CAS No. 207802-45-7) is proposed as a novel dye for LIF thermometry in liquid flows. RuPhen has been used previously in the form of a temperature-sensitive gel (Lam et al. (2012)), and also in temperature sensitive paints (TSPs). RuPhen is found to be well suited for this work as it has a peak absorption at 470nm as shown in Fig. 2a and more importantly a strong temperature dependent emission mainly in the orange/red as shown in Fig. 2b (550-770 nm). Similar to Rhodamine B (RhB), the fluorescence emission of RuPhen is decreasing with temperature and seems to not have a temperature-dependent absorption coefficient, $\epsilon(T)$ (Fig. 2a), but rather its quantum yield $\phi(T)$ is most likely changing with temperature. Temperature sensitivity, s as described in Chaze et al. (2016), for RuPhen is found to be -4%/$^{\circ}C$ as shown in Fig. 2d which is more than twice when that of RhB (Fig. 2c). Fig. 2d also shows that the temperature sensitivity of RuPhen over the emission wavelength is almost constant, hence the red and green channels of the color camera capture almost the same reduction in the fluorescence signal over different temperatures. As a low-cost alternative to a standard pulsed laser, a continuous wave (CW) laser is

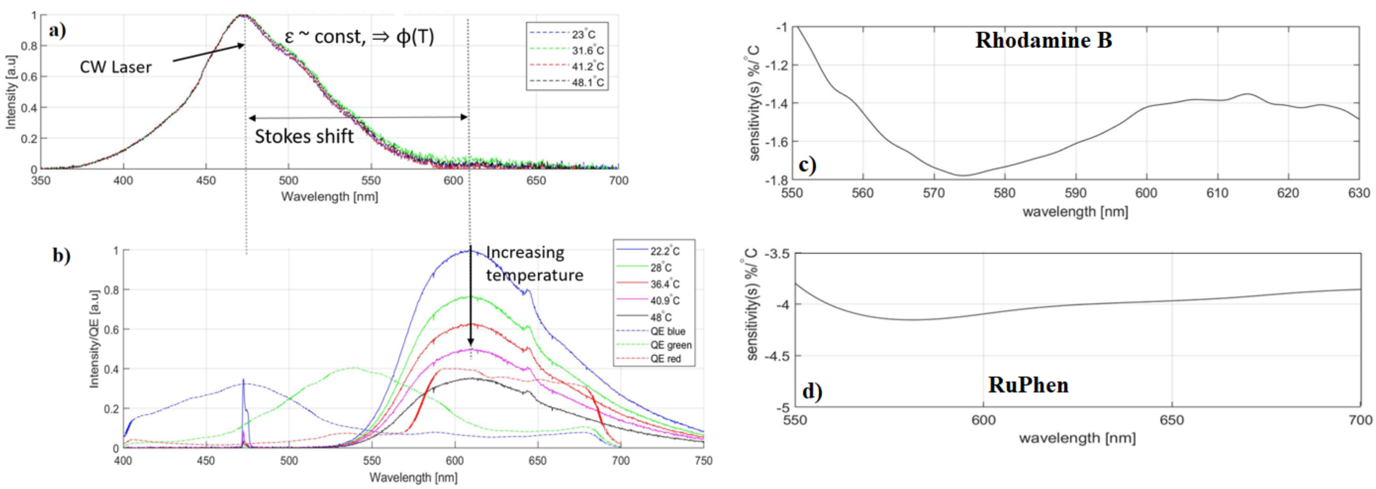

Figure 2. RuPhen absorption (a), emission spectra at different temperatures along with QE curves of the PCO Edge sCMOS sensor (b), and temperature sensitivity coefficient, s, for (c) Rhodamine B and (d) RuPhen

assembled that is based on a 3.5W laser diode module from OSRAM operating at λ_e=465nm (cost of laser diode : 300 CHF). The laser diode is mounted on a thermoelectric cooling (TEC) element and attached to a diode driver/TEC controller inside a housing as shown in Fig. 3a. A light sheet

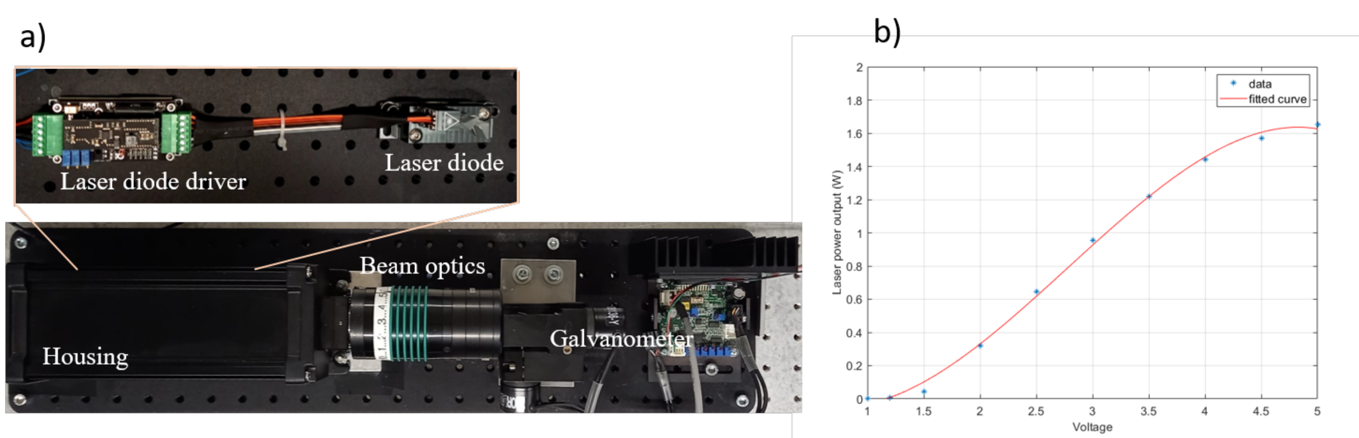

Figure 3. a) Photograph of the CW laser showing the laser diode, beam optics and a galvanometer, and b) measured laser power output vs voltage for the CW laser

optics module is used to form a laser sheet and a Thorlabs galvanometer (GVS 012, scan rate up to a 1kHz for small angles) is used to scan the light sheet in order to extend the technique to 3D-LIF/3D-2C PIV. The laser can also be modulated up to 500kHz and the measured power for an input voltage of 0-5V is shown in Fig. 3b. We use a CW laser so as to excite the dye in the weak excitation limit where the laser irradiance is much less than the dye saturation limit ($I_0 << I_{sat}$, Chaze et al. (2016)) and thus the fluorescence signal is linearly proportional to the laser irradiance,

I_0. Our aim is to measure velocity and temperature fields over a field-of-view (FOV) of $\approx 150 \times 150 \times 50$ mm^3 where volume illumination cannot be used as the laser sheet when expanded to such a volume would lead to poor signal-to-noise ratio mainly in LIF images due to lower power associated with CW lasers. An alternative solution would require an expensive setup consisting of a pulsed laser, and several intensified cameras for tomographic reconstruction (for example see the study by Halls et al. (2016) in case of a gaseous free jet). Therefore, a scanning laser sheet remains the only viable option for our low-cost 3D LIF setup wherein we obtain single-shot instantaneous temperature fields with a sufficiently high signal-to-noise ratio.

4. Calibration and correction for laser power fluctuations

Channels/combination ratios normalized by a reference temperature ($R_n, G_n, R_n/G_n, R_nG_n/B_n^2$) all show a monotonous decrease with temperature albeit with varying temperature sensitivity as shown in Fig. 4. These can be used to derive a 3rd-degree polynomial calibration curve that relates the intensity values to temperature. The main challenges in LIF are the apparent intensity fluctu-

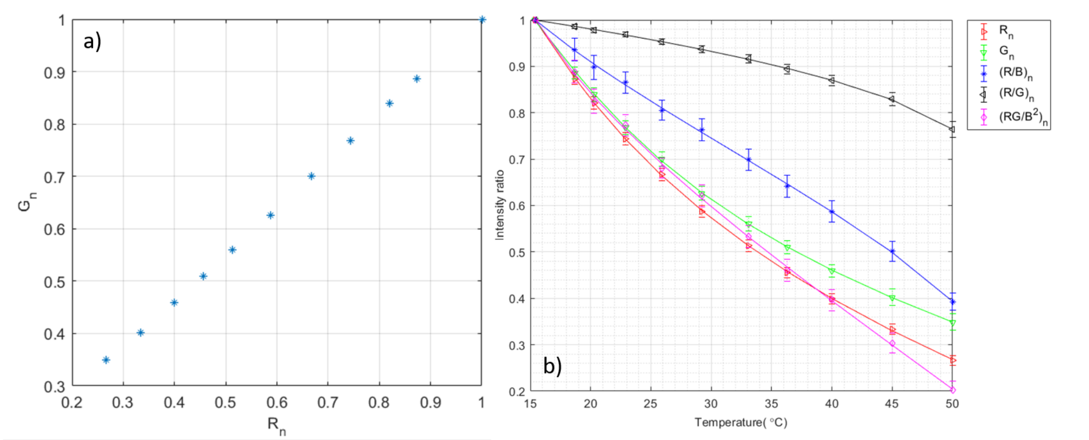

Figure 4. a) Correlation of the R and G channels, and b) temperature calibration of various ratios

ations that are not due to temperature changes. Using two channels i.e ratios R_n/G_n or R_nG_n/B_n^2 helps to correct the three main error sources i.e. non-uniform laser sheet profile, laser fluctuations and the weak absorption. However, the use of green and blue channels is not ideal due to the contribution of laser illumination and the Mie-scattering of particles that are difficult to remove, ultimately adding considerable noise to the temperature fields. Moreover, since the red and green channels are highly correlated (Fig. 4a), the ratio R_n/G_n decreases the temperature sensitivity as can be seen clearly in Fig. 4b. Normalizing the red channel with a reference temperature i.e. R_n has the advantage of high-temperature sensitivity and a clear separation between the fluorescence emission and laser irradiance (hence independent of the seeding concentration). R_n also corrects for the non-uniform laser sheet profile and the weak absorption. In the following section, we present a method to eliminate the laser fluctuations $I_0(t)$ using both the red and green channels.

Consider a camera signal S, gain G, dark level D, observed light intensity I, temperature T and recording time t, we have,

$$S(x, y, T, t) = G(x, y)I(x, y, T, t) + D(x, y) \tag{1}$$

For low concentrations, dye absorption can be neglected (optically thin system assumption $C\epsilon(\lambda_f)L_{obs} << 1$ Walker (1987)), the fluorescence intensity received by the sensor (I_r) is in the form:

$$I_r(x, y, T, t) = I_0(t)L(x, y)F(x, y, T) \tag{2}$$

where I_0 is the time dependent laser intensity, L(x,y) is the light sheet non-uniformity, and F is the fluorescence signal.

The ratio of full camera image w.r.t recording at uniform reference temperature is:

$$\rho(x, y, T, T_{ref}, t, t_{ref}) = \frac{S(x, y, T, t) - D(x, y)}{S(x, y, T_{ref}, t_{ref}) - D(x, y)} \tag{3}$$

Substituting equation 5.1 and 5.2, we get,

$$\rho(x, y, T, T_{ref}, t, t_{ref}) = \frac{I_0(t)F(x, y, T)}{I_0(t_{ref})F(x, y, T_{ref})} \tag{4}$$

Relative red and green signals on separate pixels of Bayer pattern lead to:

$$\rho_R(x_R, y_R, T, T_{ref}, t, t_{ref}) = \frac{I_0(t)F(x_R, y_R, T)}{I_0(t_{ref})F(x_R, y_R, T_{ref})} \tag{5}$$

$$\rho_G(x_G, y_G, T, T_{ref}, t, t_{ref}) = \frac{I_0(t)F(x_G, y_G, T)}{I_0(t_{ref})F(x_G, y_G, T_{ref})} \tag{6}$$

These signals are dependent on the current laser intensity ratio $\Gamma = I_0(t)/I_0(t_{ref})$, which remains unknown in each frame (i.e. at every time t) but is the same for all color channels. The intensity ratio Γ can be determined by considering multiple measurements with given pairs $\{\rho_R, \rho_G\}$ in each separately recorded frame. Given a large number of pixel-based values of the red and green channels, the equal temperature criteria can be used to find the best estimate for the global intensity ratio Γ. For a specific exponential model we can obtain,

$$\rho_R(T) = \Gamma(\alpha_R + \beta_R exp[-\gamma_R(T - T_0)]) \tag{7a}$$

$$T = T_0 - \frac{1}{\gamma_R} ln\left(\frac{\rho_R/\Gamma - \alpha_R}{\beta_R}\right) \tag{7b}$$

$$\rho_G(T) = \Gamma(\alpha_G + \beta_R exp[-\gamma_G(T - T_0)]) \tag{8a}$$

$$T = T_0 - \frac{1}{\gamma_G} ln\left(\frac{\rho_G/\Gamma - \alpha_G}{\beta_G}\right) \tag{8b}$$

$$\sum \left| \frac{1}{\gamma_R} ln \left(\frac{\rho_R/\Gamma - \alpha_R}{\beta_R} \right) - \frac{1}{\gamma_G} ln \left(\frac{\rho_G/\Gamma - \alpha_G}{\beta_G} \right) \right| \rightarrow min \quad (9a)$$

The global value for Γ can then be used to compute T from ρ_R alone which is the most reliable measurement, here

$$T = T_0 - \frac{1}{\gamma_R} ln \left(\frac{\rho_R/\Gamma - \alpha_R}{\beta_R} \right) \quad (10)$$

In the exponential model the estimate for Γ can be derived independent of the actual local temperature. Thus, it can be obtained also for single-shot images while different temperatures are present in the camera's field of view. In the case of Ruphen dye, the calibration curves of normalized red and green responses are shown in Fig. 5a. Assuming a 10% variation in the laser power during the measurements, the uncorrected temperature estimate is shown in Fig. 5b and the result after applying the above correction model using R, G channels is shown in Fig. 5c.

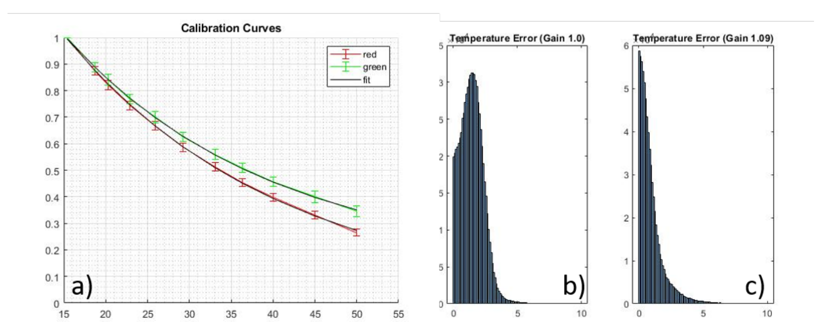

Figure 5. a) Temperature calibration curves using normalized red and green channels b) histogram showing the bias error due to 10% variation in laser power and c) corrected histogram after applying laser power correction

5. 3D LIF/3D2C PIV Experimental Setup

We demonstrate our technique by performing simultaneous PIV-LIF measurements in the refractive index matching (RIM) water tunnel (test section: 15 cm × 15 cm × 38 cm) at the Swiss Federal Laboratories for Material Science and Technology (Empa). We quantify the nature of the flow both inside and around a heated hollow hemisphere in various flow regimes ranging from natural to forced convection. The model consists of a circular heater from Minco (diameter 5 cm, model: HM6970), and the transparent hemisphere is manufactured by thermoforming a fluorinated ethylene propylene (FEP) sheet (Fig. 6). With the refractive index (RI) of FEP (RI: 1.3385) is very close to water, a 5% by wt. glycerol solution is added to match the RI of water with FEP. A concentration of 0.2 ppm (2.8E-7 mol/l) of RuPhen is used as the temperature sensitive fluorescent LIF dye along with hollow glass spheres (HGS, size:10μm) as tracers for the PIV measurement. The measurement setup consists of the CW laser assembly (λ_e = 465 nm) as the excitation source for RuPhen and a

PCO "edge 5.5" color sCMOS camera (single frame, 50mm lens, aperture F/2.8) that is placed perpendicular to the light sheet (Fig. 6). The Mie-scattering of PIV particles is captured in the blue channel, whereas the temperature-dependent fluorescence signal is registered in the red channel of the camera. A Fresnel lens corrects for the small-angle deviations produced by the Galvanometer

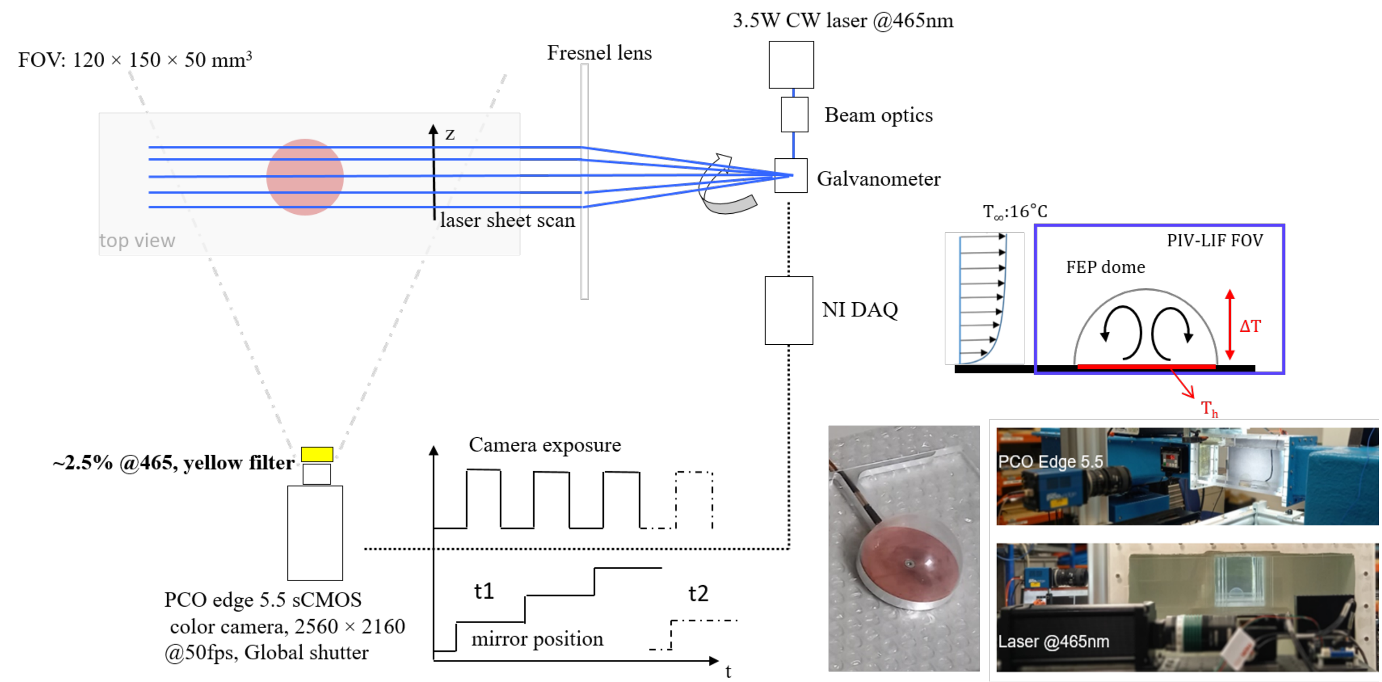

Figure 6. Schematic diagram of the experimental setup and photographs of the water tunnel setup, and the circular heater/ FEP dome assembly

to render the laser sheets parallel. Yellow filters (2 × Schott GG475, transmittance: 2.5% @ 465nm) are used in front of the camera to avoid overexposing the blue channel and any subsequent leakage to the red/green channels. Images are acquired using an in-house Matlab/C++ script that synchronizes the laser pulse, the galvo position and the PCO edge camera using a National Instruments data acquisition device, NI-USB-6221. The tunnel is cooled using a Lauda VC5000 to obtain in-situ uniform temperature LIF calibration images with the same field-of-view as the final measurements.

6. Results and discussion

6.1. Application demonstration: Thermal plume

For early validation, 3D LIF measurements are carried out using a 25 l aquarium. A square heated plate model consisting of a heating element from Minco is used as a simple test case (similar set up as shown in Fig. 6). A concentration of 0.1 ppm (1.4E-7 mol/l) of RuPhen is used along with hollow glass spheres (HGS) 10m particles. We quantify the 3D temperature field of a thermal plume over a 50mm square heated plate at T=50$^{\circ}C$, FOV: 12 × 15 × 5 cm^3). To set a surface temperature, a

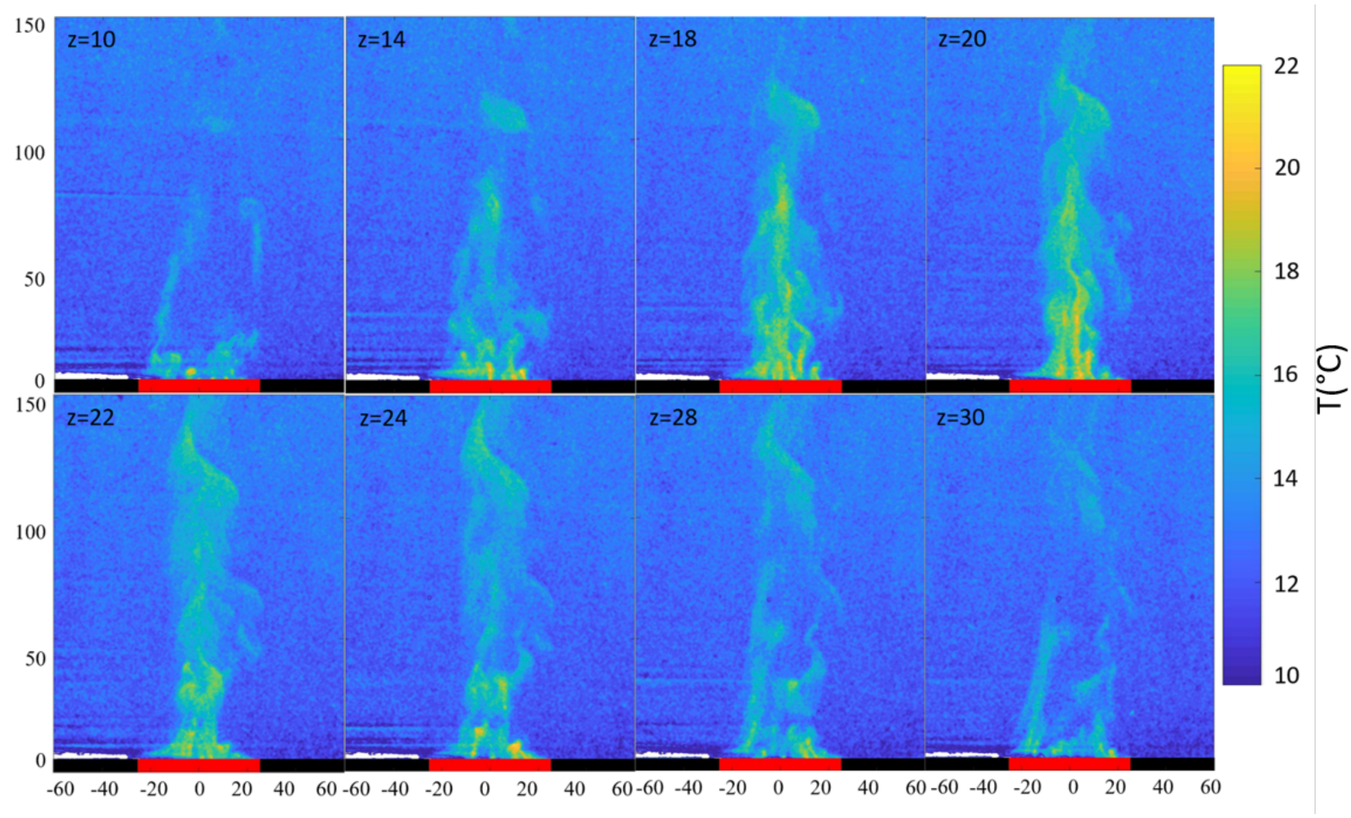

Figure 7. Snapshots of 'single-shot' temperature fields of the turbulent thermal plume obtained at various depth distances by a scanning laser sheet

temperature controller is used along with a T-type thermocouple as a reference and a data logger from Sefram. Measurements are carried out at an acquisition frequency of 62Hz, lens aperture 2.8, and scanning $z = 40$ planes. Instantaneous temperature fields of the thermal plume for various z-planes are shown in Fig. 7 where the development of the turbulent thermal plume is clearly seen.

6.2. Application demonstration: Flow past and inside a heated hollow hemisphere

The mean temperature and velocity fields at mid-plane at different flow regimes for the heated hollow hemisphere case are shown in Fig. 8. The bulk temperature field measured using LIF is relatively uniform, especially outside the dome, and is validated with thermocouple measurements. In case of natural convection, a symmetric large-scale recirculation pattern induced by thermal convection and a thermal boundary layer are established. The results clearly show the effects of cross-flow on the recirculation inside the hemisphere. Due to differences in the heat transfer rates upstream and downstream of the dome, an asymmetric pattern in the large-scale recirculation region is observed in the velocity field (for Ri >1). The downstream thermal boundary layer and the temperature in the shear layer are also visualized and quantified for the high Richardson number cases (Ri >1). Interestingly, this asymmetric recirculation pattern becomes symmetric again for Ri < 0.01 (forced-convection regime) as the enhanced mixing in the turbulent near wake leads to comparable heat transfer rates in the downstream region. The LIF temperature field also indicates the expected cooling at the outer edges and in the regions where large-scale recirculation occurs.

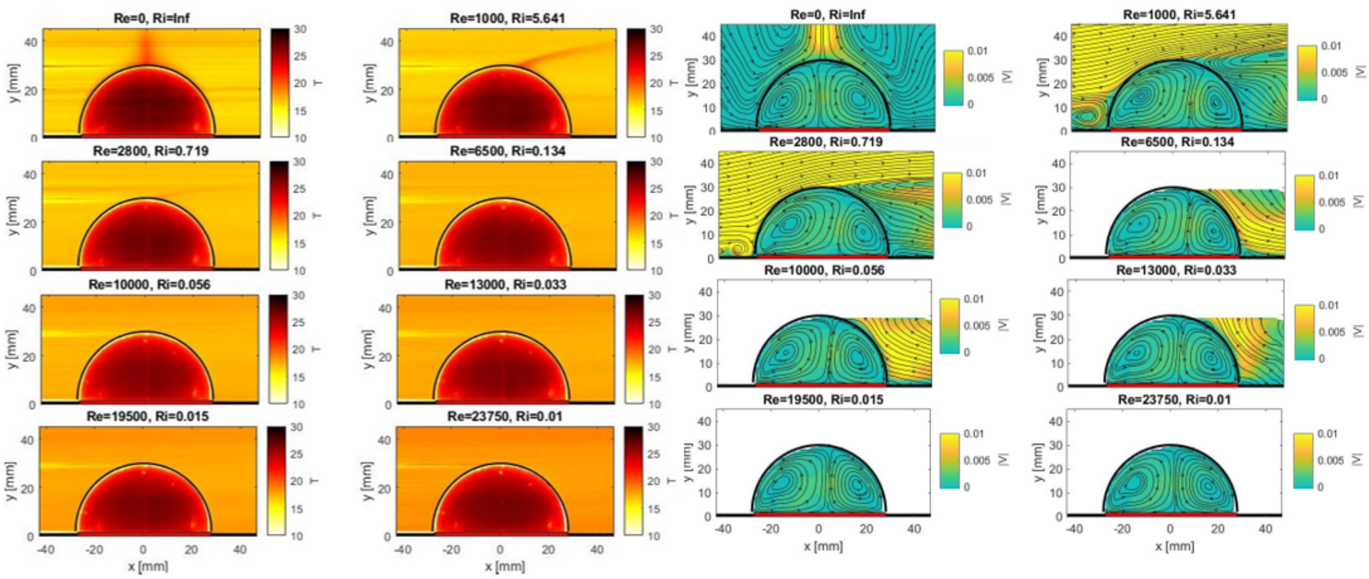

Figure 8. Mean temperature and velocity fields at various Re, Ri numbers for the heated hemisphere case

7. Conclusions

In this study, we evaluated the combination of a single color sCMOS camera, a low-cost CW laser system, and a novel dye RuPhen to simultaneously measure temperature and velocity fields. The technique could also be extended to 3D LIF/3D-2C PIV by incorporating a scanning light-sheet using a galvanometer. We show that only a low concentration of the RuPhen dye is required because of the strong absorption at 465nm and as a result, we are within the optically thin system limit of Walker. Also, by using RuPhen alone, i.e. a 2c/1d method, on one hand, we avoid spectral conflicts that arise in the 2c/2d techniques, and on the other hand, we have a higher temperature sensitivity coefficient (s) of up to -4%/°C that is comparable to the ones obtained in 2c/2d approaches. We observe that the red channel of the color sCMOS camera can separate the laser irradiance and dye fluorescence emission quite well. We then propose a method to use the red and green channels to correct for any laser power fluctuations. Finally, we demonstrate 3D LIF temperature measurements using a test case of a thermal plume over a heated plate and 2D LIF/PIV measurements of the flow past and inside a heated hollow hemisphere.

Acknowledgements

This research was funded by the school board and the Institute of Fluid Dynamics (IFD) at ETHZ. We thank Rene Holliger, Jovo Vidic at IFD, and Beat Margelisch, Stephan Kunz at Empa for the support with the experimental setup. We thank Christian Egli, Fabio Meier for their technical support at RAPLAB, ETHZ. We are also grateful for the use of the GVS012 Galvanometer from the Advanced Interactive Technologies (AIT) lab at ETHZ.

References

Abram, C., Pougin, M., & Beyrau, F. (2016). Temperature field measurements in liquids using zno thermographic phosphor tracer particles. *Experiments in Fluids*, *57*(7), 1–14.

Aldén, M., Omrane, A., Richter, M., & Särner, G. (2011). Thermographic phosphors for thermometry: a survey of combustion applications. *Progress in energy and combustion science*, *37*(4), 422–461.

Cellini, F., Peterson, S. D., & Porfiri, M. (2017). Flow velocity and temperature sensing using thermosensitive fluorescent polymer seed particles in water. *International Journal of Smart and Nano Materials*, *8*(4), 232–252.

Chaze, W., Caballina, O., Castanet, G., & Lemoine, F. (2016, 4). The saturation of the fluorescence and its consequences for laser-induced fluorescence thermometry in liquid flows. *Experiments in Fluids*, *57*. doi: 10.1007/s00348-016-2142-8

Coppeta, J., & Rogers, C. (1998). Dual emission laser induced fluorescence for direct planar scalar behavior measurements. *Experiments in Fluids*, *25*, 1-15.

Dabiri, D. (2009). Digital particle image thermometry/velocimetry: a review. *Experiments in Fluids*, *46*(2), 191–241.

Dabiri, D., & Gharib, M. (1991). Digital particle image thermometry: The method and implementation. *Experiments in Fluids*, *11*, 77-86.

Funatani, S., Fujisawa, N., & Ikeda, H. (2004). Simultaneous measurement of temperature and velocity using two-colour lif combined with piv with a colour ccd camera and its application to the turbulent buoyant plume. *Measurement Science and Technology*, *15*(5), 983.

Halls, B. R., Thul, D. J., Michaelis, D., Roy, S., Meyer, T. R., & Gord, J. R. (2016). Single-shot, volumetrically illuminated, three-dimensional, tomographic laser-induced-fluorescence imaging in a gaseous free jet. *Optics express*, *24*(9), 10040–10049.

Lam, H., Kostov, Y., Tolosa, L., Falk, S., & Rao, G. (2012). A high-resolution non-contact fluorescence-based temperature sensor for neonatal care. *Measurement Science and Technology*, *23*(3), 035104.

Massing, J., Kaden, D., Kähler, C., & Cierpka, C. (2016). Luminescent two-color tracer particles for simultaneous velocity and temperature measurements in microfluidics. *Measurement Science and Technology*, *27*(11), 115301.

Massing, J., Kähler, C. J., & Cierpka, C. (2018). A volumetric temperature and velocity measurement technique for microfluidics based on luminescence lifetime imaging. *Experiments in Fluids*, *59*(11), 1–13.

Schiepel, D., Schmeling, D., & Wagner, C. (2016). Simultaneous velocity and temperature measurements in turbulent rayleigh-bénard convection based on combined tomo-piv and pit. In *Proceedings of the 18th international symposium on application of laser and imaging techniques to fluid mechanics. lisbon, portugal* (pp. 4–7).

Shah, J., Allegrini, J., & Carmeliet, J. (2018). Ratiometric-2dye-lif using non-toxic dyes for temperature measurements in large-scale water tunnels. In *Proceedings of the 19th international symposium on application of laser and imaging techniques to fluid mechanics. lisbon, portugal.*

Someya, S., Li, Y., Ishii, K., & Okamoto, K. (2011). Combined two-dimensional velocity and temperature measurements of natural convection using a high-speed camera and temperature-sensitive particles. *Experiments in fluids*, *50*(1), 65–73.

Vogt, J., & Stephan, P. (2012). Using microencapsulated fluorescent dyes for simultaneous measurement of temperature and velocity fields. *Measurement Science and Technology*, *23*(10), 105306.

Walker, D. A. (1987). A fluorescence technique for measurement of concentration in mixing liquids. *J. Phys. E: Sci. Instrum*, *20*.

Westerweel, J. (1997). Fundamentals of digital particle image velocimetry. *Measurement science and technology*, *8*(12), 1379.

Willert, C. E., & Gharib, M. (1991). Digital particle image velocimetry. *Experiments in Fluids*, *10*, 181-193.